Unsupervised Classification of Polarimetric SAR Images via Riemannian Sparse Coding

Neng Zhong, Wen Yang, *Senior Member, IEEE,* Anoop Cherian, Xiangli Yang, Gui-Song Xia, *Senior Member, IEEE,* Mingsheng Liao

***Abstract*—Unsupervised classification plays an important role in understanding polarimetric synthetic aperture radar (PolSAR) images. One of the typical representations of PolSAR data is in the form of Hermitian positive definite (HPD) covariance matrices. Most algorithms for unsupervised classification using this representation either use statistical distribution models or adopt polarimetric target decompositions. In this paper, we propose an unsupervised classification method by introducing a sparsity based similarity measure on HPD matrices. Specifically, we first use a novel *Riemannian sparse coding* scheme for representing each HPD covariance matrix as sparse linear combinations of other HPD matrices, where the sparse reconstruction loss is defined by the Riemannian geodesic distance between HPD matrices. The coefficient vectors generated by this step reflects the neighborhood structure of HPD matrices embedded in the Euclidean space and hence can be used to define a similarity measure. We apply the scheme for PolSAR data, in which we first over-segment the images into superpixels, followed by representing each superpixel by an HPD matrix. These HPD matrices are then sparse coded, and the resulting sparse coefficient vectors are then clustered by spectral clustering using the neighborhood matrix generated by our similarity measure. Experimental results on different fully PolSAR images demonstrate the superior performance of the proposed classification approach against the state-of-the-art approaches.**

***Keywords*—Polarimetric synthetic aperture radar, unsupervised classification, Riemannian sparse coding, sparse induced similarity**

I. Introduction

The fully Polarimetric Synthetic Aperture Radar (PolSAR) is a technology for long-term monitoring of the Earth's surface based on multi-dimensional measurements via transmitting microwave pulses with two distinct orthogonal polarizations. The PolSAR system has beeen used in numerous remote sensing applications [1] [2] [3], because it can operate both during day and night, as well as in all weather conditions. Further, it also provides the ability to capture the geometrical structure and geophysical properties of terrain objects. In this paper, we address unsupervised classification of PolSAR images, which is an important PolSAR application.

A. Motivation and Objective

Classification of PolSAR images [1] [4] [5] is an active research topic in SAR applications. Various algorithms have been proposed for supervised and unsupervised classification in the last decades. Supervised approaches need annotated data samples to train a classifier [6], which might be expensive or challenging to obtain. Compared against supervised schemes, the unsupervised ones do not need annotated training samples, but use implicit information among the samples. Practically, limited number of labelled data might not provide sufficient support for learning an appropriate classification model [5], and thus we resort to unsupervised techniques.

In recent years, sparse representation theory has achieved great success for land cover classification in the field of remote sensing [7] [8]. Graph-based classification methods have also been found to be useful in interpreting PolSAR images and are seen to perform better than the traditional Wishart classifier [5] [9]. However, previous methods based on sparse representations, such as [5] [8], need to extract several polarimetric features first, which may lead to loss of useful information in the PolSAR data [7]. In addition, the classification performance strongly depends on what kinds of features are used– choosing the right features is a challenging practical problem. A natural question is why not use sparse coding on covariance matrices directly, which is the main motivation for the approach in this paper. For graph-based classification methods, an important difficulty is to choose the appropriate similarity measure to compute the affinity structure of the data. Combining these two ideas, we propose a novel unsupervised PolSAR image classification framework based on the recently proposed Riemannian sparse coding objective [10] and the new sparsity induced similarity measure [11].

B. Related Work

1) Unsupervised classification methods for PolSAR images: Unsupervised PolSAR image classification algorithms can be roughly categorised into two types. The first type is based on the analysis of the polarimetric scattering mechanisms. This

The research was partially supported by the National Natural Science Foundation of China (Grant No.61331016 and No.61271401) and the National Key Basic Research and Development Program of China under Contract 2013CB733404. Dr. Cherian is funded by the Australian Research Council Centre of Excellence for Robotic Vision (project number CE140100016).

N. Zhong and X. L. Yang are with School of Electronic Information, Wuhan University, Wuhan 430079, China. *E-mail: zn_whu@whu.edu.cn; xiangliyang@whu.edu.cn*

W. Yang is with School of Electronic Information and Collaborative Innovation Center of Geospatial Technology, Wuhan University, Wuhan 430079, China. *E-mail: yangwen@whu.edu.cn*

A. Cherian is with Australian Centre for Robotic Vision, Australian National University, Australia. *E-mail: anoop.cherian@gmail.com*

G.-S. Xia and M. S. Liao are with the State Key Laboratory for Information Engineering in Surveying, Mapping and Remote Sensing (LIESMARS), Wuhan 430072, China and also with the Collaborative Innovation Center of Geospatial Technology, Wuhan University, Wuhan 430079, China. *E-mail: guisong.xia@whu.edu.cn; liao@whu.edu.cn*

kind of approach can preserve physical scattering characteristics of the data. In the algorithm proposed by Van Zyl [12], the polarization properties of pixels in a PolSAR image are compared with simple classes of even number of reflections, odd number of reflections, and diffusion scattering. Many subsequent algorithms combined polarimetric target decomposition techniques and statistical distribution models, such as the classic H/α-Wishart classifier [13], the H/α/A-Wishart classifier [14], and the Freeman-Wishart classifier [4], which have been applied to various remote sensing applications.

The second category of techniques for PolSAR image classification uses clustering analysis and image processing . Jäger et al. [15] combined graph-cut optimization with expectation maximization (EM) in their classification scheme. Erashin et al. [16] introduced spectral graph partitioning into segmentation and classification of PolSAR data. Wang et el. [17] combined the tensor space cluster analysis and Markovian framework in their segmentation algorithm. Compared to these prior methods, the new method in this paper operates without manually selecting the feature vectors from covariance matrices, which provides robust classification performance for various PolSAR images.

2) Sparse representation for PolSAR images: In the past several decades, sparse representation theory has shown great promise in the field of PolSAR image interpretation. Xu et al. [18] achieved good performance in speckle reduction of PolSAR image using sparsity. In [19] and [20], sparse compression schemes are used to classify ships in high resolution TerraSAR-X images. Zhang et al. [8] presented an approach for supervised classification of PolSAR image using the sparsity on polarimetric features. However, the sparse representation methods [5] [8] need to extract several features manually, which leads to the loss of information. In computer vision domain, Harandi et al. [21] dealt with the problem of sparse coding and dictionary learning on Riemannian manifolds by embedding the manifolds into a reproducing kernel Hilbert space (RKHS). By using the Stein kernel [22] for this embedding, Yang et al. [7] first successfully applied a sparsity based classifier to multi-frequency polarimetric SAR land-cover classification problem. To discover the structure of PolSAR data in a high dimensional reproducing kernel Hilbert space, Song et al. [23] further use sparse subspace clustering techniques and present an effective approach for PolSAR image classification. Different from these methods of using feature vectors or kernel Hilbert spaces, we directly represent the covariance matrix as sparse linear combinations of other covariance matrices and adopt Riemannian sparse coding for classification of PolSAR images [24].

3) Similarity measures for PolSAR data: Hermitian positive definite covariance is one of the popular ways to represent polarimetric information of multi-look processed PolSAR images. In order to classify the pixels in these images effectively, several distance measures for comparing such covariance matrices have been introduced. In the literature [25], a large variety of distances have been discussed for various PolSAR applications. In addition to the similarity based on pixels, Deledalle et al. [26] used the patch similarity in the processing the SAR images. Based on the logarithmic likelihood function of complex Wishart distribution model, Lee et al. [13] introduced the Wishart distance and proposed a maximum likelihood classifier. Furthermore, Frery et al. [27] discussed the common form of four stochastic distances and derived their analytic expressions between relaxed complex Wishart distributions. Symmetric revised Wishart distance was proposed by Anfinsen et al. [28] to measure the pairwise similarity between different pixels for spectral clustering. By taking advantage of statistical hypothesis test theory, Kersten et al. [29] proposed Bartlett distance to measure the similarity of two covariance matrices. In addition, Song et al. [30] applied the Bartlett distance in unsupervised classification for large scale PolSAR images. Song et al. [31] combined the Jensen-Bregman LogDet Divergence (also called Stein divergence) [32] with k-means for unsupervised classification.

C. Contributions of This Work

In this paper, a PolSAR image unsupervised classification method based on Riemannian sparse coding is proposed. For each superpixel generated by the over-segmentation of a PolSAR image, we construct an associated HPD covariance matrix. Such HPD matrices are represented as sparse linear combination of matrices from other superpixels. Then, we introduce a sparsity based similarity measure between different superpixels and construct an affinity matrix. Finally, spectral clustering is employed on this affinity matrix to obtain the classification. The major contributions of our work can be summarized along two different axes as follows:

- To decompose the covariance matrix, we introduce Riemannian sparse coding using a dictionary, where each atom of this dictionary is an HPD matrix. This differs from the approach in [10] where they use a symmetric positive definite matrix instead.
- To compare the pairwise similarity between two covariance matrices, we propose a sparse induced similarity measure.

The remainder of this paper is organized as follows. In Section II, we start by reviewing the necessary background on polarimetric SAR data and the similarity measures. In section III, we describe the details of proposed method for unsupervised classification. The experimental results and discussions are provided in Section IV and we conclude in Section V.

II. Preliminaries

A. Polarimetric SAR Data

For monostatic PolSAR measurements of a reciprocal medium, the polarimetric information can be represented by a complex vector

$$\boldsymbol{k} = \left[S_{hh}, \sqrt{2}S_{hv}, S_{vv}\right]^T, \tag{1}$$

where h and v denote the horizontal and vertical wave polarization states, and ^{T} indicates vector transposition. In order to reduce the speckle noise, PolSAR data are often multilook processed. Each such data point can be represented by a polarimetric covariance matrix:

$$\boldsymbol{C} = \frac{1}{N}\sum_{i=1}^{N}\boldsymbol{k}_i\boldsymbol{k}_i^H = \begin{bmatrix} \langle|S_{hh}|^2\rangle & \sqrt{2}\langle S_{hh}S_{hv}^*\rangle & \langle S_{hh}S_{vv}^*\rangle \\ \sqrt{2}\langle S_{hv}S_{hh}^*\rangle & \langle|S_{hv}|^2\rangle & \sqrt{2}\langle S_{hv}S_{vv}^*\rangle \\ \langle S_{vv}S_{hh}^*\rangle & \sqrt{2}\langle S_{vv}S_{hv}^*\rangle & \langle|S_{vv}|^2\rangle \end{bmatrix}, \quad (2)$$

where * denotes the complex conjugation, ^{H} denotes the Hermitian transpose, and N is the number of looks.

The covariance matrix $\mathbf{C}$ can be modeled by a complex Wishart distribution in homogeneous regions of the multilook PolSAR image [33]. Assume that $\mathbf{\Sigma} = \mathbf{E}\{\mathbf{k}\mathbf{k}^H\}$, the probability density function for $\mathbf{C}$ is

$$p_C(\mathbf{C}|n,\Sigma) = \frac{n^{np}\,|\mathbf{C}|^{n-p}}{\Gamma_d(n)\,|\mathbf{\Sigma}|^n}\exp\left\{-n\mathrm{tr}\left(\mathbf{\Sigma}^{-1}\mathbf{C}\right)\right\}, \quad (3)$$

$$\Gamma_p(n) = \pi^{\frac{p(p-1)}{2}}\prod_{i=1}^{p}\Gamma(n-i+1),$$

where $\mathrm{tr}(\cdot)$ is the trace operator on a matrix, n is the number of looks and $\Gamma(\cdot)$ is the gamma function. For the fully polarimetric SAR data, the value of p is 3 with the consideration of reciprocity.

B. Similarity Measure on PolSAR Data

As one of the widely used data forms, the multilook processed polarimetric covariance matrices are Hermitian positive definite matrices, which forms a Riemannian manifold instead of a Euclidean space [10]. The similarity between two data points embedded in the Riemannian manifold can be measured by the geodesic distance.

For SPD matrices $\boldsymbol{X}$ and $\boldsymbol{Y}$ which are in the Riemannian manifold, two well-known geodesic distances are: (i) the affine invariant Riemannian metric (AIRM) [34], and (ii) the Log-Euclidean Riemannian metric (LERM) [35]. The corresponding defined functions of those two geodesic distances are respectively:

$$d_R(\boldsymbol{X},\boldsymbol{Y}) = \left\|\log(\boldsymbol{X}^{-\frac{1}{2}}\boldsymbol{Y}\boldsymbol{X}^{-\frac{1}{2}})\right\|_{\mathrm{F}}, \quad (4)$$

$$d_L(\boldsymbol{X},\boldsymbol{Y}) = \|\log(\boldsymbol{X}) - \log(\boldsymbol{Y})\|_{\mathrm{F}}. \quad (5)$$

Both these distances induce a Riemannian geometry; the former induces a curved geometry while the latter "flattens" the manifold by mapping into the tangent space at identity (which is Euclidean). LERM, however, is not affine invariant, but is rotation and scale invariant separately. While, these distances are defined for SPD matrices, their geometry naturally extends to the HPD case [36].

To further reduce the computational load, the Bartlett distance has been proposed, which is a statistically motivated similarity measure based on Bregman divergences [32]:

$$d_B(\boldsymbol{X},\boldsymbol{Y}) = \log\left|\frac{\boldsymbol{X}+\boldsymbol{Y}}{2}\right| - \frac{1}{2}\log|\boldsymbol{X}\boldsymbol{Y}|. \quad (6)$$

Theoretically, it can be shown that AIRM and Bartlett distances differ by a scaling factor [21]. Note that Bartlett distance is also known as Jensen-Bregman Logdet Divergence or Stein Divergence [22].

In the framework of spectral clustering, the commonly used method to construct an affinity matrix is based on the Gaussian kernel similarity (GKS). The GKS between two data samples can be defined as

$$s\left(\boldsymbol{X_i},\boldsymbol{X_j}\right) = \exp\left(-\frac{d^2\left(\boldsymbol{X_i},\boldsymbol{X_j}\right)}{\delta^2}\right), \quad (7)$$

where the δ is the kernel width, and $d(.)$ denotes a distance, such as the Bartlett distance.

The main drawback of GKS method is that its performance is sensitive to the value of δ which is difficult to determine. In the literature, Zelnik et al. [37] proposed a way to calculate a local scaling parameter δ_i for each sample matrix $\boldsymbol{X_i}$ instead of choosing a fixed scaling parameter δ for all data. The Gaussian kernel similarity, considering the local scaling parameter, can be rewritten as follows:

$$s\left(\boldsymbol{X}_i,\boldsymbol{X}_j\right) = \exp\left(-\frac{d^2\left(\boldsymbol{X}_i,\boldsymbol{X}_j\right)}{\delta_i\delta_j}\right), \quad (8)$$

where $\delta_i = d(\boldsymbol{X}_i,\boldsymbol{X}_K)$, and $\boldsymbol{X}_K$ is the K-th nearest neighbor of matrix $\boldsymbol{X}_i$.

Of these measures, the affine invariant Riemannian metric is the only intrinsic Riemannian metric that corresponds to a geodesic distance on the manifold of HPD matrices. Thus, we use this metric in this paper.

III. PROPOSED METHODOLOGY

In this section, we describe the details of our superpixel-based unsupervised PolSAR image classification scheme. The scheme contains four steps: (i) generating superpixels, (ii) sparse coding of covariance matrix, (iii) computing a sparsity induced similarity matrix, and (iv) spectral clustering. First, an over-segmentation algorithm is implemented to generate image superpixels. Then, each superpixel is represented as a sparse linear combination of other superpixels by Riemannian sparse coding. Next, the pairwise sparsity induced similarity matrix for all superpixels is constructed based on the sparse coding coefficients. Finally, spectral clustering is performed on the similarity matrix to get the final unsupervised classification result.

A. Superpixel Generation for PolSAR data

It is well-known [1] that region-based classification is a promising scheme which considers the spatial relations between neighboring pixels to reduce speckle noise in a PolSAR image. Centralization is a commonly used approach to represent one local region. For example, we can use one average covariance matrix V_i to represent the pixels in the i-th superpixel.

In this paper, the simple linear iterative clustering (SLIC) algorithm [38] is adopted. It is a simple, but efficient approach to generate superpixels and offers flexibility with regard to

compactness and the number of superpixels it generates [30]. Each pixel in the image is iteratively assigned to different superpixels.

The introduction of superpixels to the proposed unsupervised PolSAR image classification framework can not only reduce the number of HPD matrices involved in the computation, but also implicitly integrate spatial information. Therefore, the classification process becomes more effective and the results are more interpretable.

B. Riemannian Sparse Coding for PolSAR data

Sparse coding for vector data has achieved great success and has been applied in many computer vision applications. The aim of sparse coding for vector-valued data is to find the sparsest linear combination of basic elements from an overcomplete dictionary comprised of vector data. Inspired by the work of Cherian & Sra [10] for the Riemannian sparse coding of SPD matrices, we extend this setup to HPD-valued matrices for analyzing PolSAR data [24].

Similar to the aim of sparse coding for vector-valued data, the main goal of Riemannian sparse coding for HPD-valued data is to express the given HPD matrix as sparse linear combination of basic elements from a dictionary, where each element itself is an HPD matrix.

Assume that we have a dictionary $\mathcal{B}$ comprised of HPD matrices $\{\boldsymbol{B}_1, \boldsymbol{B}_2, \ldots, \boldsymbol{B}_N\}$ as atoms and an input HPD matrix $\boldsymbol{X}$ which needs to be sparse coded. The goal of Riemannian sparse coding for matrix $\boldsymbol{X}$ is to seek a nonnegative sparse vector $\boldsymbol{\alpha} = [\alpha_1, \alpha_2, \ldots, \alpha_N]^T$, which makes the linear combination $\sum_i \boldsymbol{\alpha}_i \boldsymbol{B}_i$ as close to $\boldsymbol{X}$ (in Riemannian geodesic distance) as possible. The above sparse coding problem can be written as follows:

$$\min_{\boldsymbol{\alpha} \succeq 0} \ \phi(\boldsymbol{\alpha}) := \frac{1}{2} d^2 \left(\sum_{i=1}^{N} \boldsymbol{\alpha}_i \boldsymbol{B}_i, \boldsymbol{X} \right) + \mathrm{P}(\boldsymbol{\alpha}), \tag{9}$$

where $\mathrm{P}(\boldsymbol{\alpha})$ is the penalty term.

It has been proved in [36] that $\phi(\boldsymbol{\alpha}) := d^2 \left(\sum_i \boldsymbol{\alpha}_i \boldsymbol{B}_i, \boldsymbol{X} \right)$ is a convex function on the set:

$$\mathcal{A} := \{\boldsymbol{\alpha} | \sum_{i=1}^{N} \boldsymbol{\alpha}_i \boldsymbol{B}_i \preceq \boldsymbol{X}, \text{ and } \boldsymbol{\alpha}_i \geq 0\}, \tag{10}$$

Using the ℓ_1 norm as the sparsity penalty, we can rewrite the problem (9) as the following minimization function via replacing the distance by the affine invariant Riemannian metric:

$$\min_{\boldsymbol{\alpha} \succeq 0} \phi(\boldsymbol{\alpha}) := \frac{1}{2} \left\| \log(\sum_{i=1}^{N} \boldsymbol{\alpha}_i \boldsymbol{X}^{-\frac{1}{2}} \boldsymbol{B}_i \boldsymbol{X}^{-\frac{1}{2}}) \right\|_{\mathrm{F}}^2 + \beta \left\| \boldsymbol{\alpha} \right\|_1, \tag{11}$$

where $\beta > 0$ is a regularization parameter. The above minimization problem (11) with the constraint condition in (10) is nothing but a regularized nonnegative convex optimization problem which can be solved by the spectral projected gradient (SPG) [10].

C. Sparse Induced Similarity for PolSAR Data

The sparsity induced similarity (SIS) measure for vector-valued data was first proposed and applied in the label propagation application by Cheng et al. [11]. Here we extend this measure to HPD matrix using the sparse coefficients generated by the Riemannian sparse coding algorithm.

Assume that $\mathcal{F} = \{\boldsymbol{F}_1, \boldsymbol{F}_2, \ldots, \boldsymbol{F}_N\}$ denotes all HPD matrices in an image and $\boldsymbol{F}_k \in \mathcal{F}$ denotes the given matrix that needs to be sparse coded. We first code the HPD matrix $\boldsymbol{F}_k$ by a dictionary whose elements are the rest of the HPD matrices in $\mathcal{F}$, that is, our dictionary is composed of the set $\mathcal{F}_k = \mathcal{F} \backslash \boldsymbol{F}_k = \{\boldsymbol{F}_1, \boldsymbol{F}_2, \ldots, \boldsymbol{F}_{k-1}, \boldsymbol{F}_{k+1}, \ldots, \boldsymbol{F}_N\}$. Then, the matrix $\boldsymbol{F}_k$ can be decomposed as a sparse linear combination of $\mathcal{F}_k$. Finally, the non-negative coefficient vector of dictionary elements $\boldsymbol{\alpha}_k = [\alpha_1, \alpha_2, \ldots, \alpha_{k-1}, \alpha_{k+1}, \ldots, \alpha_N]^T$ is obtained by Riemannian sparse coding.

Once the coefficient vector $\boldsymbol{\alpha}_k$ is obtained, the sparsity-induced similarity of HPD matrix $\boldsymbol{F}_k$ with respect to $\boldsymbol{F}_i$ is defined as

$$s_{ki} = \frac{\alpha_i}{\sum_{j=1, j \neq k}^{N} \alpha_j}. \tag{12}$$

Being different with the equation (7) of literature [11], our sparse coefficient is non-negative. Therefore, it is unnecessary to use the max function in our method. After repeating this step for every HPD matrix $\boldsymbol{F}_k \in \mathcal{F}$, $k = 1, \ldots, N$, the coefficient matrix $\boldsymbol{S}_{ij} (1 \leq i, j \leq N)$ is obtained. Considering the symmetry, the final similarity matrix W is defined as

$$\boldsymbol{W}_{ij} = \begin{cases} \dfrac{\boldsymbol{S}_{ij} + \boldsymbol{S}_{ji}}{2} & (i \neq j) \\ 1 & (i = j) \end{cases}. \tag{13}$$

If the dictionary size is too large, the computational cost will become very expensive to solve the Riemannian sparse coding problem in (11) for every HPD matrix. Thus, we adopt a heuristic method which chooses the first N HPD matrices (instead of all the remaining HPD matrices) that are closest to the given matrix $\boldsymbol{F}_k$ in terms of the Bartlett distance to form the Riemannian sparse coding dictionary in our experiments.

D. Spectral Clustering for PolSAR Data

Spectral clustering algorithm is a well-known clustering method based on graph theory, which has also been widely used in unsupervised classification problems on PolSAR images. Because of its ability to cluster arbitrarily shaped data distributions, this approach can handle sample data which has relatively complex structures and unknown distribution shapes. It does not depend on estimating explicit models of cluster distributions and sample features, rather a spectral analysis of the point-to-point affinity matrix is used. The basic idea of spectral clustering algorithm is to cluster the eigenvectors of the graph Laplacian computed over the data similarity matrix. For a detailed review of this algorithm, see [39] [40].

Given a dataset $\mathcal{F} = \{\boldsymbol{F}_1, \boldsymbol{F}_2, \ldots, \boldsymbol{F}_N\}$ and an similarity matrix $\boldsymbol{W} \in \mathbb{R}^{N \times N}$ without negative elements, each entry $\boldsymbol{W}_{ij}$ defines the similarity between the samples $\boldsymbol{F}_i$ and $\boldsymbol{F}_j$. Then, a diagonal matrix termed degree matrix $\boldsymbol{D}$ can be defined,

whose entries $\boldsymbol{D}_{ii} = \sum_{j=1}^{N} \boldsymbol{W}_{ij}$. The graph Laplacian can be written as $\boldsymbol{L} = \boldsymbol{D} - \boldsymbol{W}$. Spectral clustering then seeks out the k eigenvectors which correspond to the graph Laplacian's k smallest eigenvalues for representing the original data. With those eigenvectors obtained, the classical k-means is performed to get the final clusters. There are many popular methods to solve the spectral clustering problem, such as the well-known normalized-cut algorithm [41].

IV. Experimental Results

In this section, we evaluate the performance of the proposed superpixel-based unsupervised classification scheme using different PolSAR datasets. The first dataset is an EMISAR L-band fully PolSAR image, which is acquired in Foulum area, Denmark. The second one is acquired by L-band AIRSAR sensor in Flevoland area, Netherland. The third one is also AIRSAR L-band PolSAR image acquired over from Flevoland area, Netherland.

The dataset of EMISAR is used to give a simple qualitative comparison among four approaches, i.e., the classic iterated Wishart classifier [42], the spectral clustering method based on the local scaling Gaussian kernel similarity [37] and the sparse induced similarity [11] with Hoekman feature vector [43], and the proposed method. The other two AIRSAR datasets are used to provide detailed quantitative analysis of the performances.

A. Design of Experiments

The classical Wishart classifier based on the K-means clustering algorithm (denoted by "Wishart-K") is used as the baseline for comparison. The spectral clustering method based on the Gaussian kernel similarity with automatic local scale is employed for comparison. To construct the Gaussian kernel similarity, we use the Bartlett diatance [29] to measure the similarity between superpixels (denoted by "Bartlett-SC"). We also implement the spectral clustering algorithm with sparsity-induced similarity based on Hoekman feature (denoted by "Hoekman-SIS") to compare with our similarity measure based on Riemannian sparse coding (denoted by "RSC-SIS"). The steps below outline our scheme.

First, we use the simple linear iterative clustering (SLIC) algorithm [30] [38] to generate superpixels. SLIC is an easy and efficient over-segmentation technique, which generates robust superpixels. In all our experiments, the SLIC algorithm is applied on the composite RGB image in Pauli basis ($|S_{hh} - S_{vv}|$ for red, $|S_{hv}|$ for green and $|S_{hh} + S_{vv}|$ for blue). To preserve the image boundary well and obtain good segmentation performance, we set the strength of the spatial regularization N_m as 0.1 in the stage for generating superpixels.

Second, the affinity matrix is constructed based on the similarity between different superpixels. In Riemannian sparse coding, the number of dictionary elements N_d is set empirically. We find that very small values will degrade the performance, since the PolSAR data could not be decomposed by the dictionary well with a small N_d value. For very large values, the computational complexity is high. In our experiments, we used a dictionary of fixed size, which is 10 times the HPD matrix dimensionality. Thus, the value of N_d is set as 30 considering a tradeoff between complexity and accuracy. We also select the regularization parameter as 0.1 so that the coding coefficients generated are approximately 10% sparse. The value of connectivity neighborhood parameter in "Bartlett-SC" approach is set to $R = 7$. For "Hoekman-SIS" method, the number of closest neighboring vectors is chosen as 14 as suggested in [11]. In the final stage of spectral clustering, the value of the number of clusters G needs to be specified manually.

Among existing standard distances for evaluating the clustering performance, we calculate the overall accuracy (OA), pair-counting F1-measure [44], purity, and entropy [45] to verify the performance of the proposed approach. As pointed out in [44] [45], the higher values of OA, $F1$, $Purity$ and the lower value of $Entropy$ indicate a better performance of unsupervised classification solution.

B. Experimental Results of EMISAR Data

Our first dataset is an EMISAR L-band fully PolSAR image, which is acquired from an agricultural area in Foulum, Denmark in 1998. Its number of looks is 16. The land cover types of this area include agricultural fields, forest, and several buildings. The image size is 300×150 pixels. Its composite RGB image in Pauli basis ($|S_{hh}-S_{vv}|$ for red, $|S_{hv}|$ for green and $|S_{hh}+S_{vv}|$ for blue) is shown in Fig. 1(a).

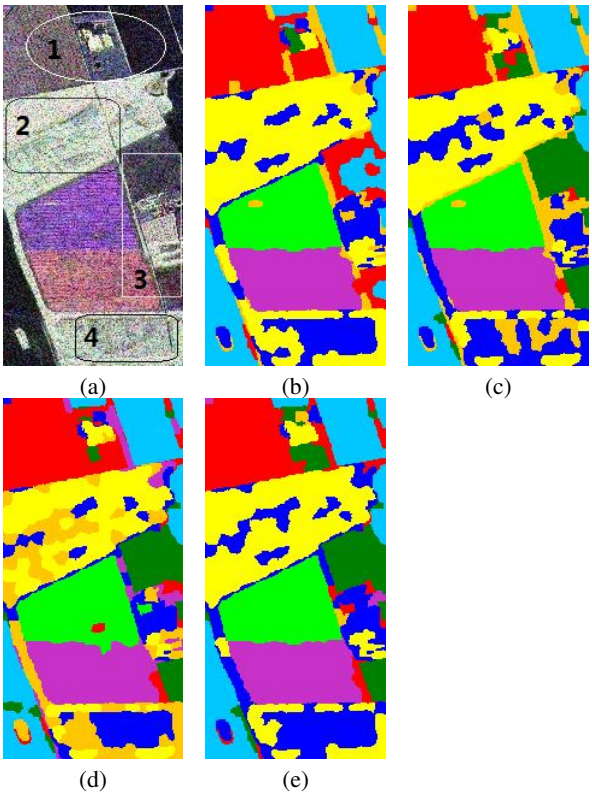

Fig. 1. EMISAR PolSAR image and clustering results. (a) RGB image in Pauli basis. (b) result of Wishart-K. (c) result of Bartlett-SC. (d) result of Hoekman-SIS. (e) result of RSC-SIS.

In the superpixels generating stage, we set the normal size of the regions N_s as 10. The results of different methods are shown in Fig. 1(b)∼(e), in which the image is clustered into 8 classes. Comparing the visualized results in the Fig. 1(b)∼(e), we can find that the "RSC-SIS" method achieves the best classification result. We marked four different regions in the composite RGB image for better comparison. In the first "Wishart-K" approach, we can observe that the classification performance is poor in heterogeneous areas, such as region 1 and region 3, from the visualized classification result shown in Fig. 1(b). Especially in region 3 the classification result is very noisy, even though the result at the top of the image is more satisfactory. In the latter "Bartlett-SC" and "Hoekman-SIS" approaches, the classification performance is lower than that of the "Wishart-K" method in the region 2 and region 4, yet we can also find that the region 3 is well separated in Fig. 1(c)∼(d). From the visualized classification results of "RSC-SIS" method shown in Fig. 1(e), it can be observed that most land cover types are well distinguished. Moreover, the "RSC-SIS" results are smoother than other three approaches, demonstrating the robustness to noise of the proposed method. In general, the visualized experimental results show the effectiveness of proposed method.

C. Experimental Results of AIRSAR Data

Our first AIRSAR data used in quantitative analysis is an L-band fully PolSAR image, which was acquired over Flevoland, Netherlands in 1989. It is a four look Stokes matrix data. This test area is located in a typical agricultural area including a variety of crops. The image size is 400×400 pixels. Its composite RGB image in Pauli basis ($|S_{hh}-S_{vv}|$ for red, $|S_{hv}|$ for green and $|S_{hh}+S_{vv}|$ for blue) is shown in Fig. 2(a). The ground truth map of tested areas is visualized in Fig. 2(b). Fig. 2(c) shows the types of crops and the corresponding colors in the ground-truth, which defines nine classes, i.e., beet, alfalfa, grass, bare land, wheat, rapeseed, potato, pea, and barley.

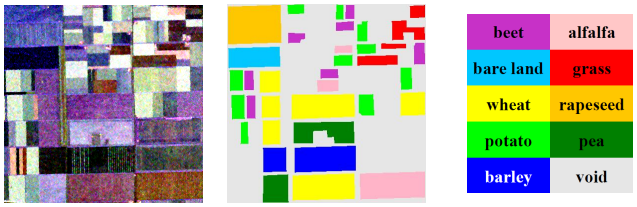

(a) (b) (c)

Fig. 2. AIRSAR, L-band, PolSAR image in Flevoland, Netherlands in 1989. (a) RGB image in Pauli basis. (b) the ground truth map. (c) the types of crops and the corresponding colors.

We set the superpixels size N_s as 10 by experience. The whole image is classificated into 9 classes and the classification results of different methods are shown in Fig. 3(a)∼(h).

From the visualized classification results shown in Fig. 3(e)∼(h), we can observe that the classification performance of the proposed method is better than other competitors. As can be seen in Fig. 3(e)∼(g), the classification results of the three former approaches are noisy in many areas,

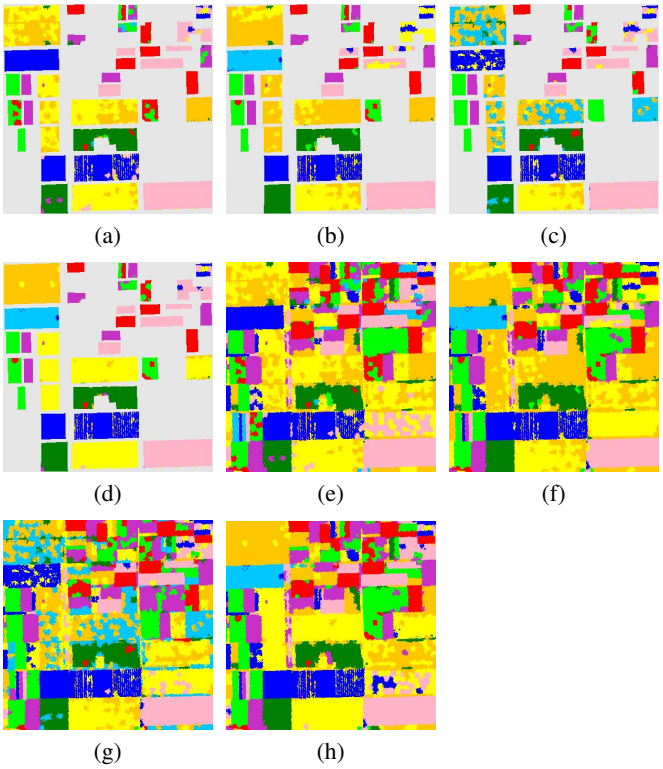

(a) (b) (c)

(d) (e) (f)

(g) (h)

Fig. 3. Clustering results of the AIRSAR data of Fig. 2. (a) result of Wishart-K. (b) result of Bartlett-SC. (c) result of Hoekman-SIS. (d) result of RSC-SIS. (e)∼(h) are the results without void mask of (a)∼(d).

and neighbouring superpixels in the same classes are classified into different groups. Since neighbouring information of superpixels are integrated via Riemannian sparse coding similarity, the classification labels of "RSC-SIS" method in Fig. 3(h) are more consistent. It also can be observed that the result of "RSC-SIS" is much smoother and more accurate than "Hoekman-SIS", demonstrating the effectiveness of directly sparse coding for PolSAR covariance matrices.

By comparing the classification results with void mask in Fig. 3(a)∼(d), it can be seen that the main agricultural land types is well classified by "RSC-SIS" method. For all four unsupervised classification methods, some potato areas are wrongly classified as grass and all grass areas are wrongly classified as other crop species. The proposed method correctly separates the areas of wheat and rapeseed, while other three methods fail. Referring to the ground truth map, the classification performance of the proposed method is improved for most crops. In particular, the classification accuracies in some areas are improved, such as wheat and rapeseed. There are fewer noisy points for the "RSC-SIS" approach in homogenous areas, than for the other three competiors. Consequently, we have demonstrated the superior robustness of our method to noise.

Table I shows the confusion matrix of the proposed method on the 1989 AIRSAR data. Table II lists the quantitative comparisons of the four unsupervised classification results,

TABLE I. CONFUSION MATRIX OF THE PROPOSED METHOD ON THE 1989 AIRSAR DATA.

	grass	potato	wheat	bare land	rapeseed	barley	beet	pea	alfalfa
grass	0	0	132	0	14	511	0	0	3807
potato	4105	4292	0	0	0	0	5	0	0
wheat	0	0	18992	0	467	0	25	37	51
bare land	0	0	1	4046	2	63	0	0	0
rapeseed	0	0	238	0	7831	0	0	0	0
barley	0	0	474	0	278	7759	36	0	0
beet	1	480	0	0	6	0	4289	0	0
pea	105	0	0	0	84	0	115	6768	0
alfalfa	0	1	13	0	15	3	0	0	8205

including the classification accuracy of land cover types, OA, $F1$, $Purity$, and $Entropy$. From Table II, it can be observed that the OA, $F1$, and $Purity$ values of "RSC-SIS" are 0.8485, 0.8633 and 0.9047, respectively. They are higher than those of other methods. At the same time, the $Entropy$ value of "RSC-SIS" is 0.1344, which is the lowest among all four classification methods. That is to say, the proposed method achieves satisfactory classification results. As described, our proposed approach obtains the best classification performance, which is not only indicated by the visual interpretation, but also can be observed by quantitative evaluation indicators.

TABLE II. PERFORMANCE EVALUATION OF THE CLASSIFICATION RESULTS OF THE 1989 AIRSAR DATA.

Method	Wishart-K	Bartlett-SC	Hoekman-SIS	RSC-SIS
grass	0	0	0	0
potato	0.3694	0.4793	0.6045	0.5108
wheat	0.6626	0.3446	0.3030	0.9704
bare land	0	0.9786	0.0005	0.9839
rapeseed	0.5162	0.7865	0.4739	0.9705
barley	0.8504	0.8982	0.8796	0.9056
beet	0.7883	0.8943	0.9056	0.8980
pea	0.9136	0.9540	0.8913	0.9570
alfalfa	0.9965	0.9843	0.9822	0.9961
OA	0.6265	0.6538	0.5598	0.8485
F1	0.6084	0.6376	0.5479	0.8633
Purity	0.7324	0.8015	0.7388	0.9047
Entropy	0.2909	0.2353	0.2930	0.1344

To further verify the effectiveness of proposed method, we carry out quantitative analysis for another PolSAR dataset. The second AIRSAR data is an L-band fully PolSAR image obtained from the Flevoland, Netherlands in 1991. It is a four look Stokes matrix data. This scene covers an agricultural land; the size of the image is 430×280 pixels. A composite RGB image in the Pauli basis ($|S_{hh}-S_{vv}|$ for red, $|S_{hv}|$ for green and $|S_{hh}+S_{vv}|$ for blue) is shown in Fig. 4(a). The ground truth map of tested areas is visualized in Fig. 4(b). Fig. 4(c) shows the types of crops and the corresponding colors in the ground truth, in which seven classes, i.e., wheat, beet, potato, grass, rapeseed, flax, and barley are defined.

Similar to the experimental steps mentioned above, we set the parameter of superpixel size in the methods as $N_s = 5$. Fig. 5(a)∼(h) show the classification results of different methods, the whole image is classified into 7 groups. By comparing the results in Fig. 5(e)∼(h), it can be concluded that the

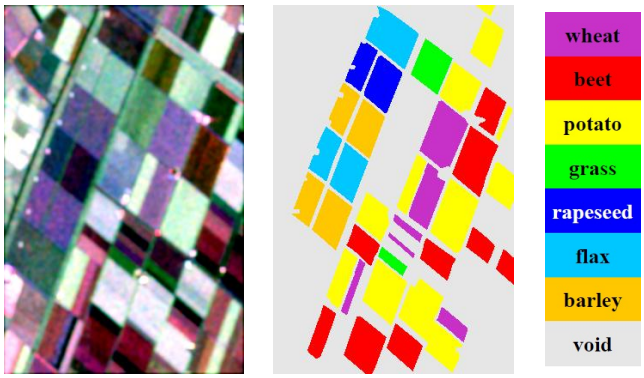

(a) (b) (c)

Fig. 4. AIRSAR, L-band, PolSAR image in Flevoland, Netherlands in 1991. (a) RGB image in Pauli basis. (b) the ground truth map. (c) the types of crops and the corresponding colors.

classification performance of the proposed method is the best on this dataset. Particularly, the classification labels of "RSC-SIS" in Fig. 5(h) are more consistent and the edges of different crops preserve well compared with that in Fig. 5(e)∼(g).

According to the ground truth map in Fig. 4(b), we can find that the classification accuracy of the proposed method is the highest among the results with void mask in Fig. 5(a)∼(d). This owes to the ability of the proposed approach to provide better similarity measures among the decomposed superpixels and their neighbors.

The confusion matrix of the proposed method on the 1989 AIRSAR data is shown in Table III. Table IV shows the quantitative comparisons of classification results, the OA, $F1$, $Purity$, and $Entropy$ values of "RSC-SIS", which are 0.9319, 0.9260, 0.9319 and 0.0979, respectively. As in the previous case, we found that the proposed approach not only achieves the highest values of OA, $F1$ and $Purity$, but also has the lowest value of $Entropy$. As expected, the visualized classification results and the quantitative evaluation indicators verify the superior performance of the proposed method.

D. Discussion

There are several technicalities in our scheme that affect the performance of unsupervised classification results. In this section, we give a brief discussion about these technicalities. One such problem is setting the parameters of the SLIC algorithm for generating superpixels. The size of segments and

TABLE III. CONFUSION MATRIX OF THE PROPOSED METHOD ON THE 1991 AIRSAR DATA.

	beet	grass	potato	falx	barley	rapeseed	wheat
beet	10198	322	4	0	0	486	0
grass	28	2049	0	0	0	108	0
potato	0	11	15871	0	0	516	0
flax	3	146	1	5155	64	18	0
barley	0	39	6	0	5805	47	0
rapeseed	0	0	0	0	0	2835	0
wheat	2	1439	0	0	0	142	4359

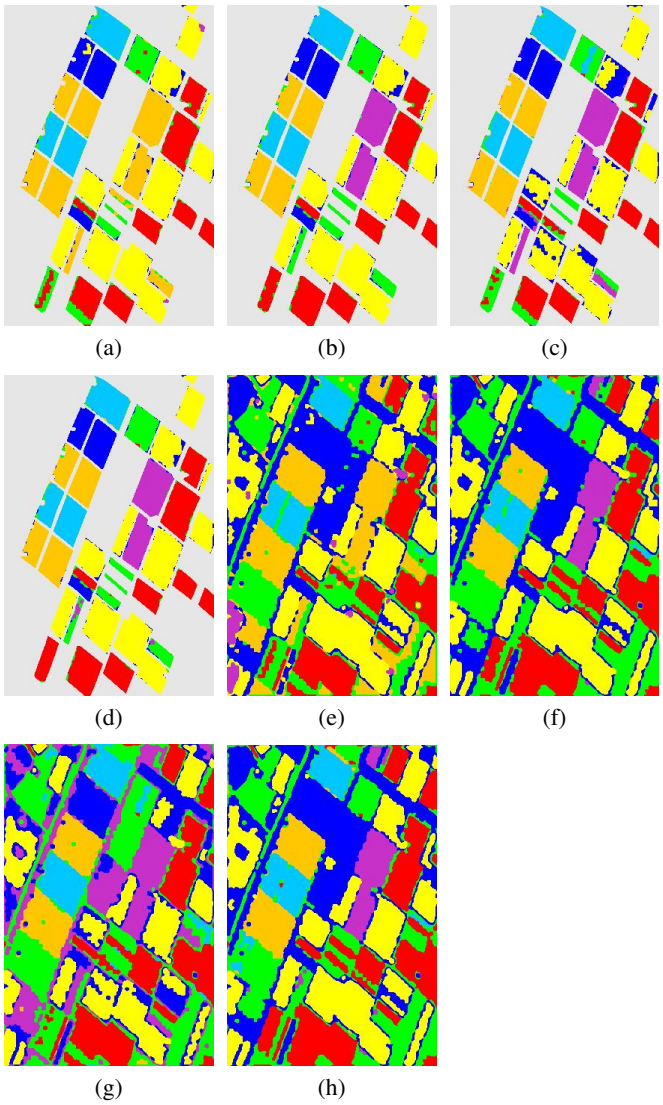

Fig. 5. Clustering results for the AIRSAR data of Fig. 4. (a) result of Wishart-K. (b) result of Bartlett-SC. (c) result of Hoekman-SIS. (d) result of RSC-SIS. (e)∼(h) are the results without void mask of (a)∼(d).

the strength of relationships between a pixel and its neighborhood should be carefully taken into account for obtaining more robust regions in the stage of generating superpixels. Here we show two results of superpixel segmentation on the

TABLE IV. PERFORMANCE EVALUATION OF THE CLASSIFICATION RESULTS OF THE 1991 AIRSAR DATA.

Method	Wishart-K	Bartlett-SC	Hoekman-SIS	RSC-SIS
beet	0.8098	0.9110	0.8083	0.9262
grass	0.9217	0.9437	0.6920	0.9378
potato	0.9671	0.9646	0.8047	0.9679
flax	0.9339	0.9504	0.9516	0.9569
barley	0.9869	0.9719	0.9847	0.9844
rapeseed	0.9619	0.9982	0.9877	1
wheat	0	0.6994	0.8480	0.7336
OA	0.8129	0.9213	0.8535	0.9319
FI	0.8471	0.9143	0.7941	0.9260
Purity	0.8148	0.9213	0.8613	0.9319
Entropy	0.1922	0.1098	0.1668	0.0979

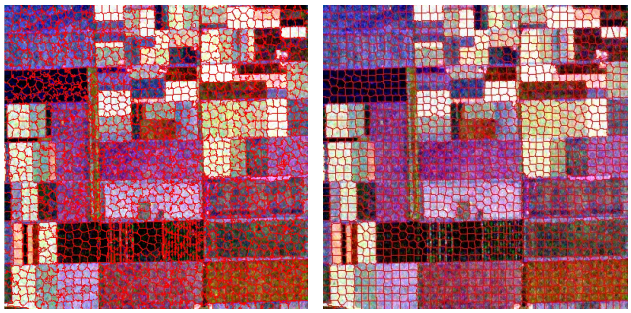

Fig. 6. The example results of superpixel segmentation on the 1989 AIRSAR data. (a) $N_s = 10$, $N_m = 0.1$. (b) $N_s = 10$, $N_m = 0.9$.

1989 AIRSAR data with different value of N_m. From the visual segmentation results in Fig. 6, we can see the SLIC algorithm can provide a relatively precise estimation of each segmentation.

Another technicality is how to adaptively determine the optimal number of neighboring superpixels to form the sparse coding dictionary; the value of which is set empirically in current method. We used a dictionary of fixed size, which is 10 times the HPD matrix dimensionality. Table V shows the computational time of Riemannian sparse coding averaged over 100 trials for different number of atoms in coding dictionary. Our implementations are in MATLAB and the timing computations used a single core Intel 3.4GHz CPU.

The computational time corresponding to each step averaged over 10 trials for three experimental images is listed in the Table VI: (i) the first step of generating superpixels by the SLIC algorithm, (ii) the second step of computing the

TABLE V. THE COMPUTATIONAL TIME OF RIEMANNIAN SPARSE CODING.

atoms	20	30	50	100	200
Time (seconds)	0.0280	0.0345	0.0462	0.0722	0.1235

Riemannian sparse induced similarity (SIS) matrix, and (iii) the final step of spectral clustering (SC).

TABLE VI. THE COMPUTATIONAL TIME OF THREE EXPERIMENTAL IMAGES.

Time (seconds)	SLIC	SIS	SC
The EMISAR data	0.3036	14.8815	0.5425
The 1989 AIRSAR data	1.6158	57.5373	3.8964
The 1991 AIRSAR data	1.8998	177.1355	82.3204

Moreover, how to automatically determine appropriate number of clusters is still an open challenging problem. For example, the joint optimization of clustering and model selection based on Boolean matrix factorization could be considered to find the optimal number of clusters. Fig. 7 shows our preliminary results on the EMISAR data using our Riemannian sparsity-induced similarity with two different methods for automatically determining the optimal number of clusters: (i)self-turning spectral clustering (STSC) [37], (ii)simultaneous clustering and model selection (SCMS) [46].

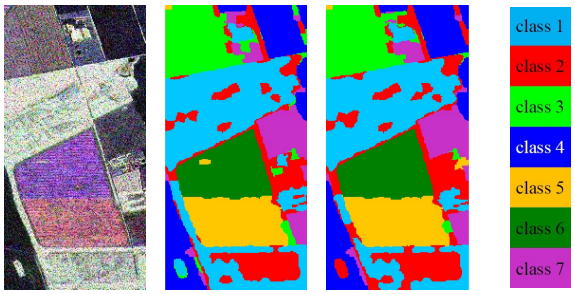

Fig. 7. Automatically determine the number of clusters on the EMISAR data. (a) RGB image in Pauli basis. (b) result of STSC. (c) result of SCMS. (d) color code.

V. CONCLUSION

In this paper, we have proposed an unsupervised PolSAR image classification method based on the Riemannian sparse coding algortihm and sparsity-induced similarity measure on the sparse coefficients. By introducing superpixels in the classification framework, the information of neighborhood pixels are implicitly intergrated. Thus, the classification process becomes more effective. The Riemannian sparse coding algorithm decomposes the HPD covariance matrices from a superpixel into a non-negative sparse linear combination of basic elements from a dictionary; this dictionary is formed by such matrices from other superpixels. The sparsity-induced similarity is employed to measure the difference between such encoded superpixels and construct the affinity matrix, which can be used in a graph-based clustering stage. The experimental results on different PolSAR images show that using our scheme is efficient and leads to superior performance against other competing methods.

ACKNOWLEDGMENT

The authors sincerely thank the anonymous reviewers, whose insightful comments and suggestions strengthened a lot this paper.

REFERENCES

[1] B. Liu, H. Hu, H. Wang, K. Wang, X. Liu, and W. Yu, "Superpixel-based classification with an adaptive number of classes for polarimetric sar images," *IEEE Transactions on Geoscience and Remote Sensing*, vol. 51, no. 2, pp. 907–924, 2013.

[2] E. Ramsey and A. Rangoonwala, "Mapping oil in a coastal marsh with polarimetric synthetic aperture radar," in *Oceans*, pp. 1–8, Hampton Roads, VA, 2012.

[3] I. Hajnsek, T. Jagdhuber, H. Schon, and K. P. Papathanassiou, "Potential of estimating soil moisture under vegetation cover by means of polsar," *IEEE Transactions on Geoscience and Remote Sensing*, vol. 47, no. 2, pp. 442–454, 2009.

[4] J.-S. Lee, M. Grunes, E. Pottier, and L. Ferro-Famil, "Unsupervised terrain classification preserving polarimetric scattering characteristics," *IEEE Transactions on Geoscience and Remote Sensing*, vol. 42, no. 4, pp. 722–731, 2004.

[5] B. Ren, B. Hou, J. Zhao, and L. Jiao, "Unsupervised classification of polarimetirc sar image via improved manifold regularized low-rank representation with multiple features," *IEEE Journal of Selected Topics in Applied Earth Observations and Remote Sensing*, no. 99, pp. 1–16, 2016.

[6] T. Zou, W. Yang, D. Dai, and H. Sun, "Polarimetric sar image classification using multifeatures combination and extremely randomized clustering forests," *Eurasip Journal on Advances in Signal Processing*, vol. 2010, no. 2, p. 9, 2010.

[7] F. Yang, W. Gao, B. Xu, and J. Yang, "Multi-frequency polarimetric sar classification based on riemannian manifold and simultaneous sparse representation," *Remote Sensing*, vol. 7, no. 7, pp. 8469–8488, 2015.

[8] L. Zhang, L. Sun, B. Zou, and W. M. Moon, "Fully polarimetric sar image classification via sparse representation and polarimetric features," *IEEE Journal of Selected Topics in Applied Earth Observations and Remote Sensing*, vol. 8, no. 8, pp. 3923–3932, 2015.

[9] K. Ersahin, I. G. Cumming, and M. J. Yedlin, "Classification of polarimetric sar data using spectral graph partitioning," in *IEEE International Geoscience and Remote Sensing Symposium*, pp. 1756–1759, 2006.

[10] A. Cherian and S. Sra, "Riemannian dictionary learning and sparse coding for positive definite matrices," *IEEE Transactions on Neural Networks and Learning Systems*, vol. PP, no. 99, pp. 1–13, 2016.

[11] H. Cheng, Z. Liu, and J. Yang, "Sparsity induced similarity measure for label propagation," in *IEEE International Conference on Computer Vision*, pp. 317–324, 2009.

[12] J. J. Van Zyl, "Unsupervised classification of scattering behavior using radar polarimetry data," *IEEE Transactions on Geoscience and Remote Sensing*, vol. 27, no. 1, pp. 36–45, 1989.

[13] J.-S. Lee, M. Grunes, T. Ainsworth, L. Du, D. Schuler, and S. Cloude, "Unsupervised classification using polarimetric decomposition and the complex Wishart classifier," *IEEE Transactions on Geoscience and Remote Sensing*, vol. 37, no. 5, pp. 2249–2258, 1999.

[14] E. Pottier and J.-S. Lee, "Unsupervised classification scheme of polsar images based on the complex Wishart distribution and the H/α/A polarimetric decomposition theorem," in *3rd European Conference on Synthetic Aperture Radar*, pp. 265–268, 2000.

[15] M. Jäger, A. Reigber, and O. Hellwich, "Unsupervised classification of polarimetric sar data using graph cut optimization.," in *IEEE International Conference on Geoscience and Remote Sensing Symposium*, pp. 2232–2235, 2007.

[16] K. Ersahin, I. G. Cumming, and R. Ward, "Segmentation and classification of polarimetric SAR data using spectral graph partitioning," *IEEE Transactions on Geoscience and Remote Sensing*, vol. 48, no. 1, pp. 164–174, 2010.

[17] Y. Wang, C. Han, and F. Tupin, "Polsar data segmentation by combining tensor space cluster analysis and markovian framework," *IEEE Geoscience and Remote Sensing Letters*, vol. 7, no. 1, pp. 210–214, 2010.

[18] B. Xu, Y. Cui, Z. Li, B. Zuo, J. Yang, and J. Song, "Patch ordering-based sar image despeckling via transform-domain filtering," *IEEE Journal of Selected Topics in Applied Earth Observations and Remote Sensing*, vol. 8, no. 4, pp. 1–14, 2014.

[19] X. Zhan, R. Zhang, D. Yin, and C. Huo, "Sar image compression using multiscale dictionary learning and sparse representation," *IEEE Geoscience and Remote Sensing Letters*, vol. 10, no. 5, pp. 1090–1094, 2013.

[20] X. Xing, K. Ji, H. Zou, and W. Chen, "Ship classification in terrasar-x images with feature space based sparse representation," *IEEE Geoscience and Remote Sensing Letters*, vol. 10, no. 6, pp. 1562–1566, 2013.

[21] M. T. Harandi, R. Hartley, B. Lovell, and C. Sanderson, "Sparse coding on symmetric positive definite manifolds using bregman divergences," *IEEE Transactions on Neural Networks and Learning Systems*, vol. 27, no. 6, pp. 1294–1306, 2016.

[22] S. Sra, "Positive definite matrices and the symmetric stein divergence," *ArXiv e-prints*, 2011. http://adsabs.harvard.edu/abs/2011arXiv1110.1773S.

[23] H. Song, W. Yang, N. Zhong, and X. Xu, "Unsupervised classification of polsar imagery via kernel sparse subspace clustering," *IEEE Geoscience and Remote Sensing Letters*, vol. PP, no. 99, pp. 1–5, 2016.

[24] W. Yang, N. Zhong, X. Yang, and A. Cherian, "Riemannian sparse coding for classification of polsar images," in *2016 IEEE International Geoscience and Remote Sensing Symposium (IGARSS)*, Beijing, China, 2016.

[25] W. Yang, H. Song, G.-S. Xia, and C. López-Martınez, "Dissimilarity measurements for processing and analyzing polsar data: A survey," in *2015 IEEE International Geoscience and Remote Sensing Symposium (IGARSS)*, pp. 1562–1565, Milan, Italy, 2015.

[26] C. A. Deledalle, L. Denis, G. Poggi, F. Tupin, and L. Verdoliva, "Exploiting patch similarity for sar image processing: The nonlocal paradigm," *IEEE Signal Processing Magazine*, vol. 31, no. 4, pp. 69–78, 2014.

[27] A. C. Frery, A. D. Nascimento, and R. J. Cintra, "Analytic expressions for stochastic distances between relaxed complex wishart distributions," *IEEE Transactions on Geoscience and Remote Sensing*, vol. 52, no. 2, pp. 1213–1226, 2014.

[28] S. N. Anfinsen, R. Jenssen, and T. Eltoft, "Spectral clustering of polarimetric sar data with the wishart-derived distance measures," in *Workshop on Science and Applications of SAR Polarimetry and Polarimetric Interferometry (POLinSAR)*, Frascati, Italy, 2007.

[29] P. R. Kersten, J. S. Lee, and T. L. Ainsworth, "Unsupervised classification of polarimetric synthetic aperture radar images using fuzzy clustering and em clustering," *IEEE Transactions on Geoscience and Remote Sensing*, vol. 43, no. 3, pp. 519–527, 2005.

[30] H. Song, W. Yang, Y. Bai, and X. Xu, "Unsupervised classification of polarimetric sar imagery using large-scale spectral clustering with spatial constraints," *International Journal of Remote Sensing*, vol. 36, no. 11, pp. 2816–2830, 2015.

[31] H. Song, W. Yang, X. Xu, and M. Liao, "Unsupervised polsar imagery classification based on jensen-bregman logdet divergence," in *2014 European Conference on Synthetic Aperture Radar (EUSAR)*, pp. 1–4, 2014.

[32] A. Cherian, S. Sra, A. Banerjee, and N. Papanikolopoulos, "Jensen-bregman logdet divergence with application to efficient similarity search for covariance matrices," *IEEE Transactions on Pattern Analysis and Machine Intelligence*, vol. 35, no. 9, pp. 2161–2174, 2013.

[33] J.-S. Lee and E. Pottier, *Polarimetric radar imaging: from basics to applications*. CRC press, 2009.

[34] X. Pennec, P. Fillard, and N. Ayache, "A riemannian framework for tensor computing," *International Journal of Computer Vision*, vol. 66, no. 1, pp. 41–66, 2006.

[35] V. Arsigny, P. Fillard, X. Pennec, and N. Ayache, "Log-euclidean metrics for fast and simple calculus on diffusion tensors.," *Magnetic Resonance in Medicine*, vol. 56, no. 2, pp. 411–21, 2006.

[36] A. Cherian and S. Sra, "Riemannian dictionary learning and sparse coding for positive definite matrices," *ArXiv e-prints*, 2015. http://arxiv.org/abs/1507.02772.

[37] L. Zelnik-Manor, "Self-tuning spectral clustering," *Advances in Neural Information Processing Systems*, vol. 17, pp. 1601–1608, 2004.

[38] R. Achanta, A. Shaji, K. Smith, A. Lucchi, P. Fua, and S. Susstrunk, "Slic superpixels compared to state-of-the-art superpixel methods," *IEEE Transactions on Pattern Analysis and Machine Intelligence*, vol. 34, no. 11, pp. 2274–2282, 2012.

[39] A. Y. Ng, M. I. Jordan, and Y. Weiss, "On spectral clustering: Analysis and an algorithm," *Proceedings of Advances in Neural Information Processing Systems*, vol. 14, pp. 849–856, 2002.

[40] U. V. Luxburg, "A tutorial on spectral clustering," *Statistics and Computing*, vol. 17, no. 4, pp. 395–416, 2007.

[41] J. Shi and J. Malik, "Normalized cuts and image segmentation," *IEEE Transactions on Pattern Analysis and Machine Intelligence*, vol. 22, no. 8, pp. 888–905, 2000.

[42] J.-S. Lee, M. R. Grunes, and R. Kwok, "Classification of multi-look polarimetric sar imagery based on complex wishart distribution," *International Journal of Remote Sensing*, vol. 15, no. 11, pp. 2299–2311, 1994.

[43] D. H. Hoekman and M. A. M. Vissers, "A new polarimetric classification approach evaluated for agricultural crops," *IEEE Transactions on Geoscience and Remote Sensing*, vol. 41, no. 12, pp. 2881–2889, 2003.

[44] A. Cherian, V. Morellas, and N. Papanikolopoulos, "Bayesian nonparametric clustering for positive definite matrices," *IEEE Transactions on Pattern Analysis and Machine Intelligence*, vol. 38, no. 5, pp. 862–874, 2016.

[45] K. Xu, W. Yang, G. Liu, and H. Sun, "Unsupervised satellite image classification using markov field topic model," *IEEE Geoscience and Remote Sensing Letters*, vol. 10, no. 1, pp. 130–134, 2013.

[46] Z. Li, L. F. Cheong, and S. Z. Zhou, "Scams: Simultaneous clustering and model selection," in *IEEE Conference on Computer Vision and Pattern Recognition*, pp. 264–271, 2014.

Neng Zhong (S'15) received the B.S. in communication engineering from Jilin University, China, in 2015.

He is currently working towards a M.S. degree in information and communication engineering at Wuhan University, China. His research involves remote sensing image processing, including classification and change detection.

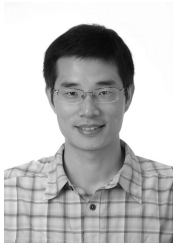

Wen Yang (M'09-SM'16) received the B.Sc. degree in electronic apparatus and surveying technology, the M.Sc. degree in computer application technology, and the Ph.D. degree in communication and information system, all from Wuhan University, Wuhan, China, in 1998, 2001, and 2004, respectively.

From September 2008 to September 2009, he worked as a Visiting Scholar with the Apprentissage et Interfaces team of the Laboratoire Jean Kuntzmann in Grenoble, France. From November 2010 to October 2013, he worked as a Postdoctoral Researcher with the State Key Laboratory of Information Engineering in Surveying, Mapping and Remote Sensing, Wuhan University. He is currently a Full Professor with the School of Electronic Information, Wuhan University. His research interests include object detection and recognition, image retrieval and semantic segmentation, multisensor information fusion, and change detection.

Anoop Cherian is a Research Fellow in the Australian Centre for Robotic Vision at the Australian National University, Canberra, Australia. He obtained his MS and PhD degrees from the University of Minnesota, Minneapolis, USA, in 2010 and 2012 respectively, after which he was a postdoctoral researcher in the LEAR project team at Inria, Grenoble, France until 2014. He obtained his Bachelors in Technology (B. Tech) degree from the National Institute of Technology, Calicut, India in 2002, later was employed at Microsoft as a software design engineer until 2007. He received the Best Student Paper Award at the International Conference on Image Processing (ICIP) in 2012 for his work on efficient similarity search on large-scale datasets. He has published nearly 40 papers in various domains including computer vision, machine learning, and robotics, at top venues such as CVPR, ICML, ICCV, ECCV, and TPAMI. His current research interests include human activity recognition, human pose estimation, modelling human-object interactions, and machine learning on matrix manifolds.

Xiangli Yang (S'16) received the M.S. in electronic and communication engineering from Wuhan University, China, in 2016.

He is currently working towards a Ph.D degree in communication and information system at Wuhan University, China. His research involves remote sensing image processing, including classification and change detection.

Gui-Song Xia (M'10-SM'15) received the B.Sc. degree in electronic engineering and M.Sc. degree in signal processing from Wuhan University, Wuhan, China, in 2005 and 2007, respectively, and the Ph.D. degree in image processing and computer vision from the CNRS LTCI, TELECOM ParisTech, Paris, France, in 2011.

Since March 2011, he has been a Post-doctoral Researcher with the Centre de Recherche en Mathmatiques de la Decision (CEREMADE), CNRS, Paris-Dauphine University, Paris, France, for one year and a half. He is currently a full Professor with the State Key Laboratory of Information Engineering, Surveying, Mapping and Remote Sensing (LIESMARS), Wuhan University, China. His current research interests include mathematical image and texture modeling, content-based image retrieval, structures from motions, perceptual grouping and remote sensing image understanding.

Mingsheng Liao received the M.Eng. degree in electronic engineering and the Ph.D. degree in photogrammetry and remote sensing from Wuhan Technical University of Surveying and Mapping (WTUSM), Wuhan, China, in 1985 and 2000, respectively.

From 1985 to 1992, he was with the Department of Electronic Engineering, WTUSM. From 1992 to 2000, he was with the State Key Laboratory for Information Engineering in Surveying, Mapping and Remote Sensing (LIESMARS), WTUSM, and obtained a Professorship in 1997. Between 1995 and 1996, he was a visiting Ph.D. candidate with the Department of Surveying and Photogrammetry, Technical University of Denmark, Kongens Lyngby, Denmark. From 2000 to 2002, he was a Research Associate with the Joint Laboratory for Geo-information Science, Chinese University of Hong Kong, Hong Kong, China. Since 2003, he has been with LIESMARS, Wuhan University, where he is leading the SAR data analysis and processing group. He has published over 100 research articles in referred scientific journals and 4 books. His research interests include interferometric and polarimetric data processing, differential SAR interferometry, and multitemporal SAR image analysis.